Nanoscale Advances

PAPER

View Article Online
View Journal | View Issue

Cite this: *Nanoscale Adv.*, 2019, **1**, 1948

Rechargeable polyamide-based *N*-halamine nanofibrous membranes for renewable, high-efficiency, and antibacterial respirators†

Ru Wang,‡[a] Yuyao Li,‡[a] Yang Si,[b] Fei Wang,[a] Yitao Liu,[b] Ying Ma,[b] Jianyong Yu,[ab] Xia Yin *[ab] and Bin Ding[ab]

Emerging infectious diseases (EIDs) have been acknowledged as a major public health concern worldwide. Unfortunately, most protective respirators used to prevent EID transmission suffer from the disadvantage of lacking antimicrobial activity, leading to an increased risk of cross-contamination and post-infection. Herein, we report a novel and facile strategy to fabricate rechargeable and biocidal air filtration materials by creating advanced *N*-halamine structures based on electrospun polyamide (PA) nanofibers. Our approach can endow the resultant nanofibrous membranes with powerful biocidal activity (6 log CFU reduction against *E. coli*), an ultrahigh fine particle capture efficiency of 99.999% (N100 level for masks), and can allow the antibacterial efficacy and air filtration performance to be renewed in a one-step chlorination process, which has never been reported before. More importantly, for the first time, we revealed the synergistic effect involving the intrinsic structure of polymers and the assembling structure of nanofibers on the chlorination capacity. The successful fabrication of such a fascinating membrane can provide new insights into the development of nanofibrous materials in a multifunctional, durable, and renewable form.

Received 20th February 2019
Accepted 24th March 2019

DOI: 10.1039/c9na00103d

rsc.li/nanoscale-advances

Introduction

Public health emergencies resulting from emerging infectious diseases, such as avian influenza, Zika, severe acute respiratory syndrome, and Ebola, have caused incalculable misery and death all over the world.[1–3] This severe issue was highlighted by the largest Ebola outbreak in West Africa with >28 000 confirmed and suspected cases and >11 000 deaths, according to the report of the World Health Organization.[4] As the front-line responders fighting against emerging infectious diseases, health care workers (HCWs) suffer from a significantly higher risk of being infected than the general population.[5,6] In the epidemic area, personal protective equipment, particularly face masks with the capability of capturing pathogens, plays a significant role in decreasing the infection incidence among HCWs.[7,8] Unfortunately, the infection cannot be completely eliminated considering the fact that the intercepted pathogens within masks remain alive, which will easily give rise to cross-contamination and post-infection.[9] Therefore, the development of materials exhibiting powerful biocidal activity is highly urgent to provide effective bioprotection for HCWs.

In response to this challenge, various antibacterial agents have been developed for application in protective masks, such as silver nanoparticles,[10,11] chitosan,[12] silk,[13] soy protein isolates,[14] *N*-halamines,[15] *etc.*, among which *N*-halamines exhibit absolute advantages over others owing to their high biocidal activity against a broad spectrum of bacteria, long-term structural stability, and rechargeable antibacterial properties.[16,17] Generally, rechargeable *N*-halamines can be formed by the substitution of hydrogen on the amide nitrogen, generating halogen atoms with a strong oxidative state, which can kill bacteria by damaging their structures.[16,18] By virtue of the desirable properties of abundant amide groups, easy accessibility, and good processibility, polyamides (PAs) have great potential for the preparation of *N*-halamine structured biocidal materials. Up to now, only a handful of efforts have been devoted to preparing PA-based *N*-halamine materials.[19–21] Worley *et al.*[19] endowed PA fabrics with antibacterial ability by hydroxymethylation, substituting oxazolidinone for the

[a]*State Key Laboratory for Modification of Chemical Fibers and Polymer Materials, College of Textiles, Donghua University, Shanghai 201620, China. E-mail: xyin@dhu.edu.cn*

[b]*Innovation Center for Textile Science and Technology, Donghua University, Shanghai 200051, China*

† Electronic supplementary information (ESI) available: Experimental setup for the evaluation of air filtration performance; a self-designed test platform for recycling filtration performance; viscosity and conductivity of PA-6, PA-66, and PA-610 solutions; morphologies of PA-6, PA-66, and PA-610 nanofibrous membranes after chlorination; the mechanical properties of PA-6, PA-66, and PA-610 nanofibrous membranes; the morphology of PA-6 nanofibrous membranes after 5 repeated quenching/chlorination cycles; clean air delivery rate of charged PA-6 nanofibrous membranes during recycling tests; the structural parameters of PA-6 nanofibrous membranes before and after chlorination. See DOI: 10.1039/c9na00103d

‡ These authors have contributed equally to this work.

hydrogen of the hydroxymethyl group, and chlorination. Obendorf *et al.*[20] prepared electrospun antibacterial PA-66 nanofibrous membranes *via* a three-step method: synthesizing a precursor (3-dodecyl-5,5-dimethylhydantoin) with N–H bonds, treating the precursor with chlorination solution to acquire *N*-halamine structures, and introducing it into a PA solution for further electrospinning. Wang *et al.*[21] fabricated a PA flat film with improved antibacterial activity and chlorine resistance *via* interfacial polymerization, synthesizing an amine functionalized hydantoin derivative, and incorporating the derivative in PA films. The fabrication of *N*-halamine structured PA membranes mentioned above is time-consuming and complicated, suggesting the urgent need for an efficient and facile strategy to fabricate PA-based *N*-halamine materials.

In addition to the powerful and rechargeable biocidal efficacy, an ideal material used for protective masks should also be equipped with excellent air filtration performance, which suggests that high particle removal efficiency and low air resistance are also of great significance to ensure the easy access to clean air for HCWs.[22–24] By virtue of the fascinating structural properties, including small fiber diameter, large specific surface area, interconnected pore structure, and easy functionalization, electrospun nanofibrous membranes (NFMs) show great promise for constructing multifunctional respirators.[25–27] Although a number of antibacterial air filters have been fabricated *via* electrospinning,[24,28,29] no effort has been devoted to the preparation of versatile and rechargeable PA-based biocidal materials used for bioprotection.

In this contribution, a novel and facile strategy for fabricating biocidal and rechargeable nanofibrous membranes is presented *via* creating an attractive biocidal structure—*N*-halamine based on electrospun polyamide (PA) nanofibers. Benefiting from the synergistic effect of the high ratio of amide bonds in the monomer and a well-manipulated nanofibrous architecture, the charged PA-6 membranes exhibited integrated properties of rechargeable chlorination capability, high biocidal efficacy, robust mechanical strength, and high and stable filtration performance. More interestingly, the membranes loaded with plenty of pollutants could recover to the clean state just by chlorination, endowing the materials with rechargeable biocidal efficacy and renewable filtration performance in one step, which, to the best of our knowledge, has never been reported before.

Experimental

Materials

Polycaprolactam (PA-6, $M_n = 18\,000$) was purchased from UBE Industries Ltd., Japan. Polyhexamethylene adipamide (PA-66, $M_n = 21\,000$) and polyhexamethylene sebacamide (PA-610, $M_n = 23\,000$) were obtained from DuPont, USA. Formic acid (>88%) (HCOOH) was bought from Shanghai Macklin Biochemical Technology Co., Ltd., China. Nonwoven substrates exhibiting negligible filtration efficiency (~3%) and pressure drop (~1 Pa) were purchased from Dalian Huayang New Material Technology Co., Ltd., China. Bleach solution containing 8 wt% free chlorine was obtained from Clorox Co., Ltd. Phosphate buffered saline (PBS) was bought from Sigma Aldrich, Germany. Agar and Luria–Bertani broth were provided by Merck Drugs & Biotechnology, Germany. *E. coli* O157:H7 (ATCC 35218) was supplied by Nanjing Lezhen Biotechnology Co., Ltd., China.

Fabrication of pristine PA NFMs

The homogeneous solutions were first obtained by dissolving PA-6, PA-66, and PA-610 particles in HCOOH at a concentration of 16 wt%, 18 wt%, and 18 wt%, respectively, with vigorous stirring for 8 hours at room temperature. Subsequently, the as-prepared solution was transferred into 5 medical plastic syringes, the tips of which were capped with metal needles to serve as the positive pole of the electrostatic field, and the solution feed rate was 0.5 mL h^{-1}. Then, the syringes were fixed in a sliding table with a moving speed of 100 cm min^{-1}. When the solution reached the needle mouth with a feed rate of 0.5 mL h^{-1}, a high voltage of 30 kV was applied, resulting in the formation of continuous jets, which would rapidly evolve into solid nanofibers after a flight of 20 cm. The resultant nanofibers were collected on a grounded roller coated with a nonwoven substrate with a rotating velocity of 50 rpm. This electrospinning experiment was carried out by using a versatile DXES-4 spinning machine (Shanghai Najie Intelligent Technology Co., Ltd., China) at a standard temperature (25 ± 2 °C) and relative humidity (50 ± 2%). Finally, the collected NFMs were dried in a vacuum oven at 60 °C for 2 h to remove any residual solvent.

Chlorination of PA NFMs

The bleach solution was diluted to acquire the chlorination solution with 500 ppm of active chlorine. At the same time, hydrochloric acid or sodium hydroxide was added to the chlorination solution to adjust its pH. For a typical chlorination process, 2 g of PA-6, PA-66, PA-610 NFMs and PA-6 microfibrous membranes (MFM) were, respectively, immersed into four chlorination solutions (100 mL) with gentle shaking for a required time. Subsequently, all membranes were washed 5 times using distilled water with the aim of removing redundant hypochlorous moieties thoroughly and were subjected to drying treatment in a vacuum oven. To confirm the complete removal of redundant hypochlorous moieties, the water used for the last rinse was titrated, and the detailed procedure could be found in Supplementary method 1.† The rechargeability test was performed by repeatedly charging PA membranes with chlorination solution first to incorporate active chlorine into PA nanofibers, then quenching any active chlorine with excess sodium thiosulfate solution (1 wt%) for 1 h. A common iodometric titration method was employed to quantify the active chlorine contents of charged PA membranes. First, 0.5 g of *N*-halamine structured PA membranes were added to 15 mL of sodium thiosulfate solution (0.001 N) with gentle shaking for 0.5 h to ensure the complete consumption of *N*-halamine, then 0.001 N iodine standard solution was added to the solution dropwise to examine the amount of residual sodium thiosulfate. According to the measured volumes (mL) of the iodine solution consumed for titrating sodium thiosulfate solution without and with charged PA membranes, denoted as V_0 and V_s,

respectively, and the weight (g) of the PA membranes (m_s), the active chlorine content (ppm) of PA membranes could be determined by $34.45 \times (V_0 - V_s) \times 500/m_s$.

Antimicrobial assays of PA NFMs

Bactericidal experiments started with the cultivation of typical etiological bacteria; 10 mL of fresh broth was prepared for the inoculation of *E. coli* O157:H7, and the suspension was cultivated in an incubator at 37 °C. After 24 h, the suspension was centrifuged at 5000 rpm for 5 min for harvesting the *E. coli*. After that, the obtained *E. coli* was washed 3 times with PBS and diluted in deionized water or in nutrient broth solutions with a chemical oxygen demand (COD) of 1000 to realize a concentration of 1×10^8 CFU mL^{-1}. In a typical bactericidal test, control films (pristine PA membranes) or charged PA membranes were cut into square pieces with a size of 2×2 cm^2 and placed inside a plastic Petri dish. Then, 10 μL of the *E. coli* suspension was dripped on the top surface of the as-prepared samples with a contact time of 5, 10, 20, 30, 40, 50, and 60 min. At each point of time, the membranes loaded with 10 μL of *E. coli* suspension were placed into a glass tube with 1 mL of deionized water by using small tweezers. Following an oscillating process for 30 s, the bacteria were detached from the membranes completely (Fig. S1†). Then, the mixture was serially diluted ($\times 10^2$, $\times 10^3$, $\times 10^4$, and $\times 10^5$), and 100 μL of which was, respectively, plated on nutrient broth agar for bacteria counts. Cyclic antimicrobial assays were carried out by recharging the bacteria loaded films with chlorination solution for 1 h and after the active chlorine was completely quenched by bacteria the bacterial enumeration was finished.

Characterization of the membranes

The primary morphologies were characterized by using a scanning electron microscope (SEM, TM 3000, Hitachi Ltd., Japan HQ). In addition, the distribution of pore size was examined by a bubble point method employing a capillary flow porometer (CFP-1100AI, Porous Materials Inc., USA). The porosity of the PA NFMs was determined using the density of various raw materials (ρ_0) and fibrous membranes (ρ_1) according to the following formula:

$$\text{Porosity} = \frac{(\rho_0 - \rho_1)}{\rho_0} \times 100\%$$

The mechanical properties were obtained on a tensile tester (XQ-1C, Shanghai New Fiber Instrument Co. Ltd. China). In addition, the wicking height was measured by dipping a strip of the membrane (200 mm × 25 mm) into distilled water, which contained blue ink for tracking the movement of water according to AATCC TM 197 with modification.[30] The air filtration performance, including filtration efficiency toward particles with the most penetrable size (0.3 μm) and pressure drop, was obtained by using an LZC-H filter tester produced by Huada Filter Technology Co., Ltd., China. The measurement was carried out under an air flow velocity of 85 L min^{-1} and the detailed working principle of this machine is provided in Fig. S2.† With respect to the long-term filtration performance toward fine particles with the diameter less than 2.5 μm ($PM_{2.5}$), a simulated test was carried out by using a self-designed test platform, which is depicted in detail in Fig. S3.†

Results and discussion

Rechargeable PA membranes: synthesis and structure

We designed these biocidal and rechargeable nanofibrous membranes (BR-NFMs) mainly on the basis of three criteria: (i) the raw materials should be able to provide sufficient amide groups to be chlorinated, (ii) the membranes must possess large specific surface area, small pore size and high porosity to enhance the biocidal activity and air filtration performance simultaneously, and (iii) the *N*-halamine structured membranes should achieve rechargeable biocidal activity and renewable air filtration performance in a facile way. To satisfy the first two criteria, various PA nanofibrous membranes were fabricated and the dependence of performance on the multilevel structure involving polymers and fiber assemblies was investigated. The third requirement was achieved by a facile chlorination treatment.

Fig. 1a depicts the synthesis pathway of BR-NFMs. PA was selected for preparing porous NFMs by virtue of its easy-to-electrospun characteristic and abundant amide groups, at which the halogenation could readily take place, converting the nitrogen–hydrogen bonds (N–H) into highly biocidal nitrogen–halogen bonds. Even though halogens include chlorine, bromine, and iodine, chlorine was utilized in this work considering the fact that the bromine and iodine bonds are easier to dissociate from the membranes than chlorine, causing unstable biocidal activity.[31] The as-prepared PA NFMs were immersed into a solution containing 500 ppm of sodium hypochlorite, resulting in the formation of nitrogen–chlorine bonds (N–Cl). When the BR-NFMs come into contact with bacteria, the N–Cl group can play a role of oxidizing agent to oxidize chemical groups in bacterial cells (*e.g.* sulfides in proteins), finishing the translation of N–Cl to N–H bonds.[32,33] Therefore, the biocidal activity could be recharged by directly exposing the membrane to free chlorine in aqueous media.

Based on the fact that the molecular structure of PA has an enormous effect on the biocidal activity, three typical polymers including PA-6, PA-66 and PA-610 were electrospun considering their different carbon : nitrogen ratios and polymerization patterns of monomers. The representative SEM images of the three pristine PA NFMs shown in Fig. 1b–d exhibit a typical 3D structure comprising randomly deposited nanofibers in the form of nonwoven fabric, which could provide not only large specific surface area and small pore size for particle capture but also abundant porous channels for air transmission.[34,35] Obviously, the nanofibers obtained from PA-6, PA-66, and PA-610 presented a slightly increased diameter of 193, 203, and 211 nm, respectively (Fig. 1e). This phenomenon was contributed by the elevated viscosity and diminished conductivity of PA solutions (Fig. S4†), which would dramatically restrain the elongation of charged jets during electrospinning.[36,37] In

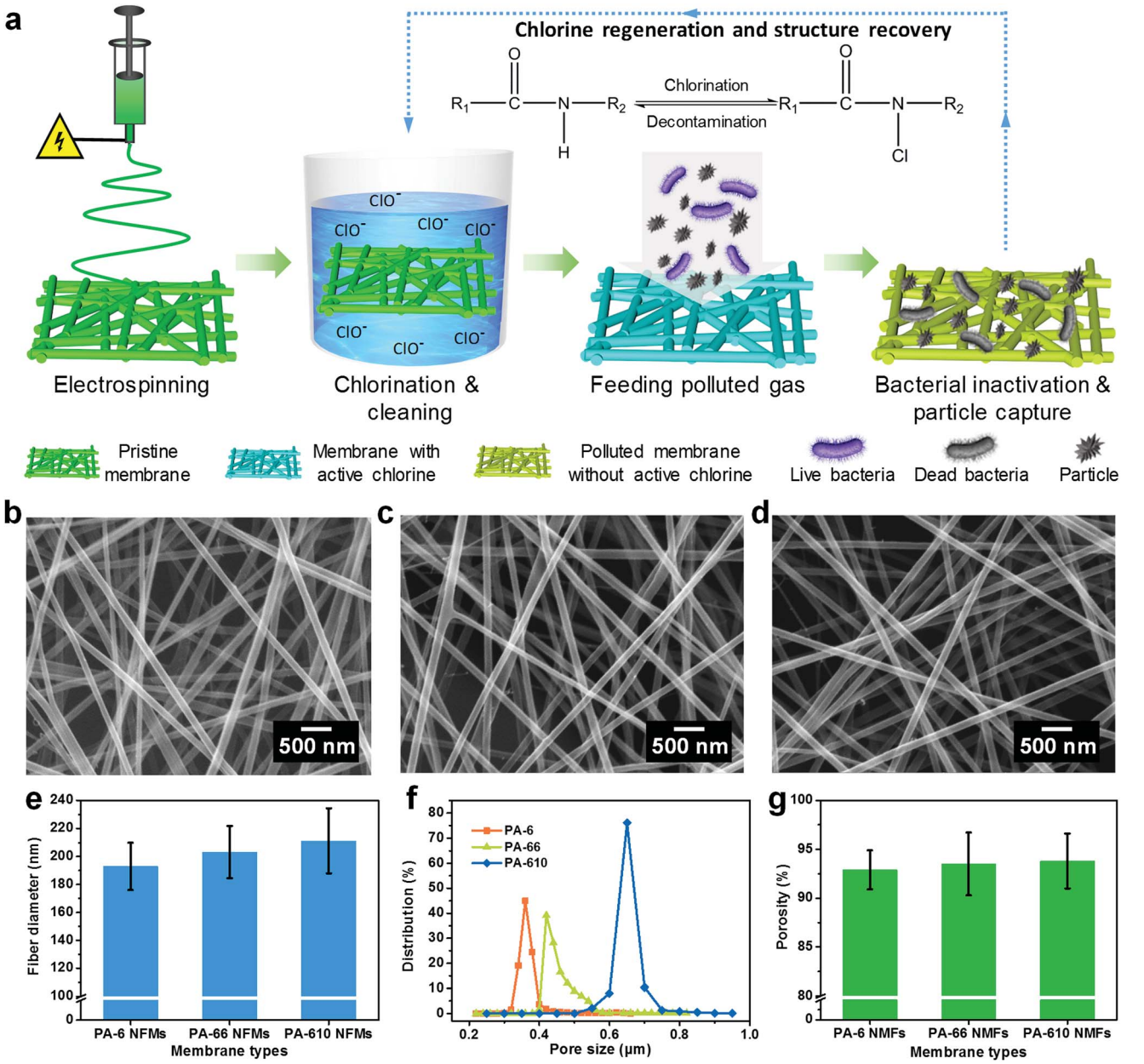

Fig. 1 (a) Schematic illustration of the design process of the versatile NFMs with rechargeable biocidal capacity and renewable air filtration performance. SEM images of pristine (b) PA-6, (c) PA-66, and (d) PA-610 NFMs. (e) Fiber diameter, (f) pore size, and (g) porosity of various PA membranes.

addition, the porous structure of different PA membranes was also evaluated by investigating their pore size and porosity, as shown in Fig. 1f and g. Evidently, both the pore size and porosity increased with the increase of fiber diameter, which was in accordance with the acknowledged point that large fiber diameter tended to result in a low amount of fibers per unit of weight, thereby generating large pores and a loosely packed structure.[38,39] Significantly, when these PA membranes were subjected to chlorination treatment, the typical 3D structure with interconnected channels could still remain intact, which could be ascribed to their sufficient mechanical properties (Fig. S5 and S6†).

Rechargeable chlorination of PA NFMs

In order to evaluate the chlorination capability, an easily accessible chlorine source—bleach solution was diluted to obtain a chlorination solution with an active chlorine content of 500 ppm, in which the pristine PA membranes were immersed and the active chlorine content of charged PA NFMs was determined using an acknowledged iodometric titration method.[32] Plotting the curves of active chlorine content of PA-6, PA-66, and PA-610 membranes *versus* chlorination time revealed three typical reaction regions: a fast linear increase region for the first 20 min, a slow increase region for the following 20 min and a saturation region for the final 20 min.

The active chlorine contents of charged PA-6, PA-66, and PA-610 NFMs were 907, 854, and 829 ppm, respectively, after chlorination treatment for 1 h (Fig. 2a). The primary factor leading to this result could be the molar number of amide groups per gram of nanofibers (N), which could be calculated using $N = n/M_r$, where n is the number of amide groups and M_r represents the molar mass of monomers. This formula was obtained based on the principle that the mass of fibers was contributed by the mass of numerous macromolecules. The detailed derivation process could be found in Supplementary method 2.† Thus, the PA-6 and PA-66 NFMs presented the same N of 0.0088 mol g^{-1}, in contrast to the PA-610 NFM with a lower N of 0.0064 mol g^{-1} (Fig. 2b), which is consistent with the result that the PA-610 NFM exhibited lower active chlorine content. Interestingly, the PA-6 NFM outperformed the PA-66 NFM in spite of their equal N, which could be attributed to the underutilization of amide groups resulting from the structure of fiber assemblies. As a proof of concept, the reacting ratio of all PA NFMs was calculated, showing an extremely low value of less than 1% (Fig. 2b), which implied that the chlorination occurred only on the shallow surface of fibers (Fig. 2e). Therefore, smaller fiber diameter, generally generating a larger specific surface area, was of great significance for achieving higher active chlorine content because the inner N–H bonds tended to be shielded by thick fibers.[40,41] The shielding effect was also evidenced by investigating the chlorination capacity of a commercial PA-6 MFM, which exhibited the same N as the PA-6 NFM but dramatically lower active chlorine content and reacting ratio, as shown in Fig. 2a and b. We could draw the conclusion that by virtue of the combination effect of the advantageous chemical structure and the smallest fiber diameter, the PA-6 NFM exhibited the highest active chlorine content.

Apart from the active chlorine content, the reaction rate is another important chlorination property from a practical point of view. Due to the dissatisfactory chlorination capability of PA-6 MFM, here we analyzed the reaction rate of PA-6, PA-66, and PA-610 NFMs by taking the first derivative of the curves in Fig. 2a. The deduced instantaneous reaction rates of the PA-6 NFM at 5 and 10 min were 43.9 and 40.45 ppm min^{-1}, respectively, which were higher than those of both PA-66 (41.2 and 40.4 ppm min^{-1}) and PA-610 (39.4 and 38.85 ppm min^{-1}). It should be noticed that although the difference among the three samples was hard to be found in Fig. 2a, it was highly significant considering the fact that only 0.5 ppm was enough for the degermation of a swimming pool.[42] More excitingly, in the short chlorination time of 10 min, the PA-6 NFM could be equipped with >400 ppm of active chlorine, which was equal to at least 99% of antibacterial efficiency according to Sun *et al.*,[30] indicating that the PA-6 NFM could be a cost-effective antibacterial material in the field of personal protection. The higher reaction rate of the PA-6 NFM could be ascribed to their relatively small pore size. Generally, when the membranes are immersed in a chlorination solution, smaller pores tend to generate a more remarkable wicking effect, resulting in the fast seepage of solution within the tortuous channels.[43] In this way, more fibers could come into contact with active chlorine in a unit time and achieve a higher reaction rate (Fig. 2e). As expected, the wicking heights of PA-6, PA-66, and PA-610 NFMs were 2.4, 2 and 1.8 cm, respectively, which was consistent with the variation tendency of their pore size (Fig. 2d).

It is well known that the pH value of chlorination solution plays a crucial role in the chlorination process, and therefore the active chlorine content as a function of pH was investigated by changing the pH from 2 to 12. The parabola shown in Fig. 3a

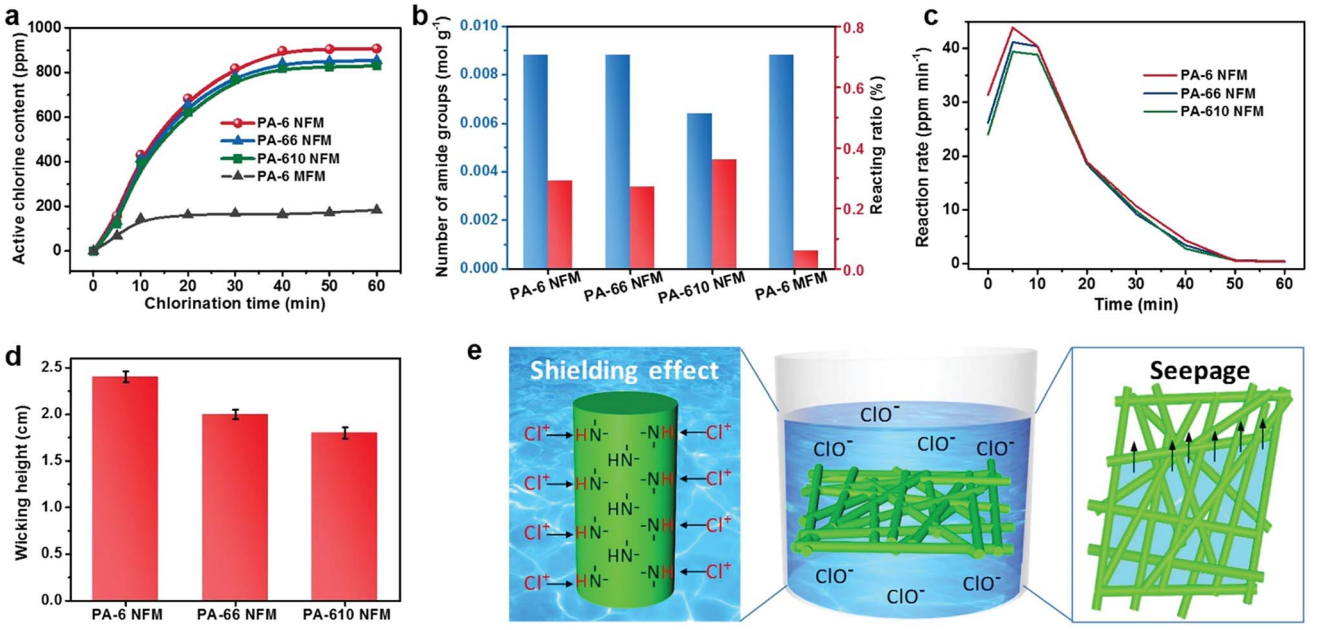

Fig. 2 (a) The variation of the active chlorine content of PA-6, PA-66, PA-610 NFMs, and the PA-6 MFM with different chlorination times. (b) The calculated number of amide groups per unit weight and the reacting ratio of amide groups. (c) Reaction rate and (d) wicking height of PA-6, PA-66, and PA-610 NFMs. (e) Schematic illustrating the synergistic effect of individual fibers and fiber assemblies on the chlorination process.

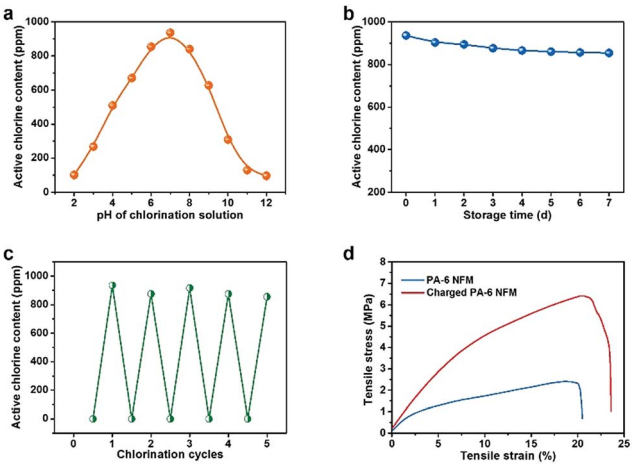

Fig. 3 Active chlorine contents of the PA-6 NFM with (a) various pH values of chlorination solutions, and (b) a long storage time. (c) The rechargeable behavior of the PA-6 NFM during repeated chlorination and quenching over 5 cycles. (d) Mechanical properties of pristine and charged PA-6 membranes.

demonstrates that the maximum efficiency was achieved around a neutral pH of 7 with the highest active chlorine content of 936 ppm, in contrast to the low active chlorine contents of ~100 ppm under acidic or alkaline conditions. This result might result from the maximum reaction rate between HOCl and –NH– under neutral conditions, further suggesting the wide range of potential applications of BR-NFMs.[44,45] Moreover, the stability of the *N*-halamine structure has a direct impact on the durability of biocidal activity, which is of great significance for practical applications. Plotting the curve of active chlorine content *versus* storage time revealed that the charged PA-6 NFM could retain >90% of the original active chlorine after 7 days, exhibiting their robust stability (Fig. 3b). Furthermore, the rechargeable function of the *N*-halamine structure was investigated by subjecting the PA-6 NFM to chlorination solution and an excess amount of thiosulfate solution repeatedly. An obvious conclusion could be drawn from Fig. 3c that the active chlorine content of the PA-6 NFM had no significant decrease even after 5 repeated quenching/chlorination cycles, which was closely associated with the sufficient tensile stress (2.4 MPa) of the PA-6 NFM to maintain the structural integrity during the cyclic test (Fig. 3d and S7†).

More excitingly, in a dramatic deviation from the already reported *N*-halamine materials exhibiting deteriorative mechanical properties after chlorination, the tensile stress was notably increased 1.6 times and the tensile strain was enhanced from 20.5% to 23.6%. Another unusual phenomenon was that the modulus of the PA-6 BR-NFM was much higher than that of the pristine PA-6 NFM, implying the decrease of toughness; however, the toughness of PA-6 tended to be enhanced when using a facile wet treatment (Fig. 3d).[46] These uncustomary results were closely related to the two-step breaking behavior of electrospun NFMs. Generally, when a small external load is applied, the randomly oriented nanofibers tend to slip and be oriented, generating the first nonlinear elastic behavior. Then, the continual increase of tensile stress would make the individual fibers elongated, generating linear elasticity. It is obvious that more cross-points among fibers would contribute to higher modulus, and tougher individual fibers could generate higher tensile stress and strain. Interestingly, the chlorination process gave rise to the contraction of area, thereby allowing more fibers to take part in the stretching process when the samples had the same test area. Moreover, benefiting from the abundant hydrophilic amide groups of PA-6, the average fiber diameter increased from 193 to 205 nm due to the swelling of nanofibers (Table S1†). Considering the structural changes of both fiber assemblies and individual fibers, the above uncustomary results of mechanical properties became reasonable. It should be mentioned that the PA-66 and PA-610 membranes presented the same mechanical enhancement phenomenon as the PA-6 NFM (Fig. S8†).

Biocidal activity against *E. coli* and air filtration performance

The high active chlorine content, stable and rechargeable *N*-halamine structure, and robust mechanical properties encouraged us to further explore the antimicrobial activity of the PA-6 BR-NFM. As the most typical etiological bacterium, *E. coli* O157:H7 was selected to evaluate the biocidal efficacy of the charged PA-6 NFM, and the microbial proliferation was quantified by agar plate assay. To obtain the biocidal efficiency, both the control and charged PA-6 NFM were loaded with 10 μL of bacterial suspension made by dispersing *E. coli* in deionized water or diluted nutrient broth with a COD of 1000. The results presented in Fig. 4a and b reveal that *E. coli* harvested from the control membranes could proliferate freely on the culture medium, and almost no biocidal activity was found. In contrast, when the COD was 0, the charged PA-6 NFM exhibited 6 log of CFU decrease with a short contact time of 10 min, which was equivalent to a high biocidal efficiency of 99.9999%. More importantly, even at a COD of 1000, the ultrahigh biocidal efficiency of 99.9999% could be realized with a contact time of 20 min, which was dramatically superior to the previous polymer films with a long contact-killing time of 5–10 h to achieve such a high biocidal efficiency.[47,48]

Inspired by their outstanding antibacterial performance, we anticipated that the PA-6 NFM could be the core material of respirators to provide bioprotection for the public and HCWs. Hence, their long-term air filtration performance was evaluated by loading particles with the most penetrable particle size of 0.3 μm for 10 h (Fig. 4c). Surprisingly, the initial filtration efficiency achieved an ultrahigh value of 99.999%, which was far higher than the required efficiency of N100 face masks (>99.97%) according to the standard of the National Institute of Occupational Safety and Health. More importantly, the antibacterial PA-6 NFM could maintain the N100 level (with a filtration efficiency of 99.988%) even after 10 h, suggesting their satisfactory filtration stability. Generally, the fresh electrospun membranes could capture particles based on the intrinsic structure and residual charges; however, the latter generally suffer from instability due to the

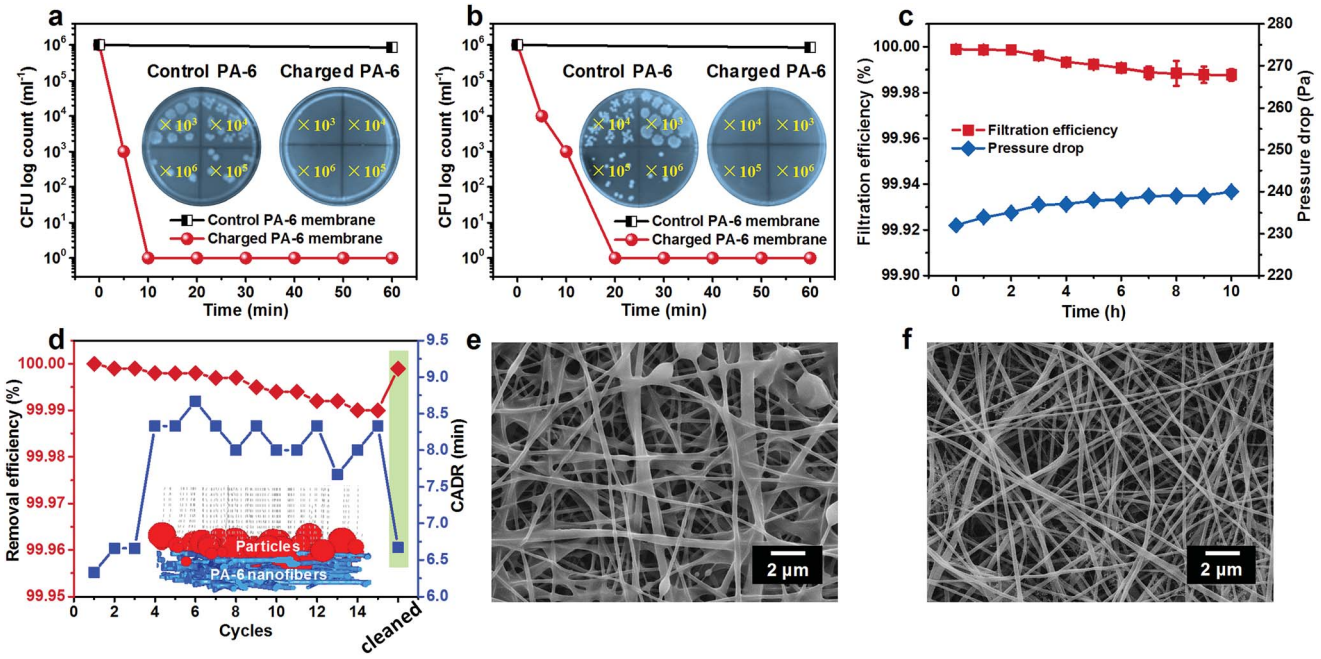

Fig. 4 Biocidal efficiency of the charged PA-6 NFM against *E. coli* O157:H7 under the conditions with COD of (a) 0 and (b) 1000. (c) Long-term filtration performance of antibacterial PA-6 membranes towards $PM_{0.3}$. (d) The removal efficiency towards $PM_{2.5}$ and the CADR of the antibacterial PA-6 NFM during 15 cycles and its reusability. The inset is the simulation of the particle capture process of antibacterial PA-6 membranes. (e) SEM image of the charged PA-6 NFM after the cyclic test. (f) SEM image of the PA-6 NFM after being cleaned using chlorination solution.

easy dissipation of charges.[49,50] Benefiting from the charge neutralization of the chlorination process, our membranes exhibited stable mechanical filtration efficiency, which could be the reason for the PA-6 NFM maintaining the N100 level in a long-term filtration process. In addition, the pressure drop showed a negligible increase (from 232 to 240 Pa), which was unfulfillable for the available materials.[37]

Furthermore, considering that the public would spend more than 90% of their time indoors, we explored the application feasibility of the PA-6 NFM in antibacterial air cleaners. Herein, the clean air delivery rate (CADR) was used to evaluate the purification power of an air cleaner and was defined as the time taken for reducing the concentration of $PM_{2.5}$ from 500 μg cm^{-3} (severe contamination level) to 35 μg cm^{-3} (good level). The test was performed in a closed cabin and the initial $PM_{2.5}$ concentration was created by burning a cigarette, as reported before.[51,52] We could draw a conclusion from Fig. 4d that the initial CADR of the charged PA-6 NFM was 6.3 min, superior to that of the already reported polyvinylidene fluoride/negative ion powder (13 min),[40] PA-6 nanofiber/nets (14.5 min),[52] and electret polyvinylidene fluoride/polytetrafluoroethylene membranes (15 min).[27] It should be mentioned that the CADR of this BR-NFM increased by 2 min and the removal efficiency towards $PM_{2.5}$ decreased from 100% to 99.99% after 15 cycles, which could be ascribed to the clogging of pores by particles. As a proof of concept, the analogue simulations of the nanofibrous filter media and particle removal process were carried out by using FiberGeo and FilterDict procedures, as presented in the inset of Fig. 4d.[53,54] According to the already obtained structural parameters involving fiber diameter, pore size, porosity, and area extension data, the 3D nanofibrous structure of the BR-NFM was cloned first. Subsequently, the filtration process was revealed by feeding a certain amount of simulated particles ranging from 0.3 to 10 μm, consistent with the particle size distribution produced by the cigarette, and tracking their paths within the porous architecture. It could be found that almost all particles were trapped owing to the large specific surface area, small pore size and tortuous channels of the BR-NFM. Moreover, it should be mentioned that most of the particles were captured on the surface of NFMs, which was typical for membrane filter media.[55] This result was also evidenced by the SEM image of charged PA-6 membranes after long-term filtration, showing that the majority of particles agglomerated on the surface and some pores were occupied by particles (Fig. 4e). Significantly, this surface filtration phenomenon made the cleaning of the BR-NFM convenient. As presented in Fig. 4f, the polluted structure could be recovered to the clean state just by immersing the membrane into the chlorination solution, and no extra cleaning agent was needed, which was superior to our previously fabricated cleanable air filters.[37] As expected, the BR-NFM presented a $PM_{2.5}$ removal efficiency of 99.999% and a CADR of 6.7 min after being cleaned by chlorination solution. Thus, our PA-6 NFM could achieve rechargeable biocidal activity and renewable air filtration performance just in one step, which, to the best of our knowledge, has never been reported before. More importantly, with the multi-needle electrospinning technology, the scale up production of the PA-6 NFM could be easily achieved (Fig. S10†).

Conclusions

In summary, *N*-halamine structured PA nanofibrous membranes were successfully fabricated to be promising candidates for antibacterial respirators through the combination of the electrospinning technique and a chlorination method. The synergistic effect of the intrinsic properties of polymers involving the monomer structure and amide ratio in the monomer, combined with the structure of nanofibrous assemblies including fiber diameter, pore size, and porosity endowed the PA-6 NFM with plenty of active sites to combine with active chlorine. The resultant membranes could kill 6 log CFU of *E. coli* in a contact time of just 10 min, maintaining the filtration efficiency of >99.97% (N100 respirator), and achieved intriguing rechargeable antibacterial efficacy and renewable filtration performance, which have been first reported to the best of our knowledge. The successful synthesis of such a multifunctional material would provide guidance for the design and fabrication of new types of respirators used in personal protective equipment.

Conflicts of interest

There are no conflicts to declare.

Acknowledgements

This work was supported by the National Natural Science Foundation of China [No. 51873031, 51673037, and 51773033], the Fundamental Research Funds for the Central Universities [DHU Distinguished Young Professor Program No. LZB2019004], and the Shanghai Committee of Science and Technology [No. 18511109500].

Notes and references

1 C. J. E. Metcalf and J. Lessler, *Science*, 2017, **357**, 149.
2 K. E. Jones, N. G. Patel, M. A. Levy, A. Storeygard, D. Balk, J. L. Gittleman and P. Daszak, *Nature*, 2008, **451**, 990.
3 L. A. Reperant and A. D. M. E. Osterhaus, *Vaccine*, 2017, **35**, 4470.
4 Ebola Situation Report, W. H. O. Ebola Virus Disease Outbreak, 2016, http://apps.who.int/ebola/current-situation/ebola-situation-report-30-march-2016.
5 S. Nuntral and A. Anucha, *Curr. Opin. Infect. Dis.*, 2015, **28**, 349.
6 D. Eibach, J.-S. Casalegno, M. Bouscambert, T. Bénet, C. Regis, B. Comte, B.-A. Kim, P. Vanhems and B. Lina, *J. Hosp. Infect.*, 2014, **86**, 188.
7 J. Gralton and M. L. McLaws, *Crit. Care Med.*, 2010, **38**, 657.
8 V. Offeddu, C. F. Yung, M. S. F. Low and C. C. Tam, *Clin. Infect. Dis.*, 2017, **65**, 1934.
9 D. Lv, M. Zhu, Z. Jiang, S. Jiang, Q. Zhang, R. Xiong and C. Huang, *Macromol. Mater. Eng.*, 2018, 1800336.
10 Y.-W. Wang, H. Tang, D. Wu, D. Liu, Y. Liu, A. Cao and H. Wang, *Environ. Sci.: Nano*, 2016, **3**, 788.
11 A. Mackevica, P. Revilla, A. Brinch and S. F. Hansen, *Environ. Sci.: Nano*, 2016, **3**, 1195.
12 M. He, H. Chen, X. Zhang, C. Wang, C. Xu, Y. Xue, J. Wang, P. Zhou and Q. Zhao, *Cellulose*, 2018, **25**, 1987.
13 G. Li, Y. Li, G. Chen, J. He, Y. Han, X. Wang and D. L. Kaplan, *Adv. Healthcare Mater.*, 2015, **4**, 1134.
14 H. Souzandeh, K. S. Johnson, Y. Wang, K. Bhanmidipaty and W.-H. Zhong, *ACS Appl. Mater. Interfaces*, 2016, **8**, 20023.
15 J. Kang, J. Han, Y. Gao, T. Gao, S. Lan, L. Xiao, Y. Zhang, G. Gao, H. Chokto and A. Dong, *ACS Appl. Mater. Interfaces*, 2015, **7**, 17516.
16 A. Dong, Y.-J. Wang, Y. Gao, T. Gao and G. Gao, *Chem. Rev.*, 2017, **117**, 4806.
17 R. Bai, Q. Zhang, L. Li, P. Li, Y.-J. Wang, O. Simalou, Y. Zhang, G. Gao and A. Dong, *ACS Appl. Mater. Interfaces*, 2016, **8**, 31530.
18 F. Hui and C. Debiemme-Chouvy, *Biomacromolecules*, 2013, **14**, 585.
19 J. Lin, C. Winkelman, S. D. Worley, R. M. Broughton and J. F. Williams, *J. Appl. Polym. Sci.*, 2001, **81**, 943.
20 K. Tan and S. K. Obendorf, *J. Membr. Sci.*, 2007, **305**, 287.
21 Y. Wang, Z. Wang and J. Wang, *J. Membr. Sci.*, 2018, **554**, 221.
22 R. Purwar, K. S. Goutham and C. M. Srivastava, *Fibers Polym.*, 2016, **17**, 1206.
23 S. Zhang, N. Tang, L. Cao, X. Yin, J. Yu and B. Ding, *ACS Appl. Mater. Interfaces*, 2016, **8**, 29062.
24 M. Zhu, J. Han, F. Wang, W. Shao, R. Xiong, Q. Zhang, H. Pan, Y. Yang, S. K. Samal, F. Zhang and C. Huang, *Macromol. Mater. Eng.*, 2017, **302**, 1600353.
25 S. Gao, G. Tang, D. Hua, R. Xiong, J. Han, S. Jiang, Q. Zhang and C. Huang, *J. Mater. Chem. B*, 2019, **7**, 709.
26 W. Ma, M. Zhang, Z. Liu, C. Huang and G. Fu, *Environ. Sci.: Nano*, 2018, **5**, 2909.
27 S. Wang, X. Zhao, X. Yin, J. Yu and B. Ding, *ACS Appl. Mater. Interfaces*, 2016, **8**, 23985.
28 C. Wang, S. Wu, M. Jian, J. Xie, L. Xu, X. Yang, Q. Zheng and Y. Zhang, *Nano Res.*, 2016, **9**, 2590.
29 K. Desai, K. Kit, J. Li, P. M. Davidson, S. Zivanovic and H. Meyer, *Polymer*, 2009, **50**, 3661.
30 Y. Si, A. Cossu, N. Nitin, Y. Ma, C. Zhao, B. Chiou, T. Cao, D. Wang and G. Sun, *Macromol. Biosci.*, 2017, **17**, 1600304.
31 Y. Si, J. Li, C. Zhao, Y. Deng, Y. Ma, D. Wang and G. Sun, *ACS Biomater. Sci. Eng.*, 2017, **3**, 854.
32 O. Gutman, M. Natan, E. Banin and S. Margel, *Biomaterials*, 2014, **35**, 5079.
33 A. Dong, S. Lan, J. Huang, T. Wang, T. Zhao, L. Xiao, W. Wang, X. Zheng, F. Liu, G. Gao and Y. Chen, *ACS Appl. Mater. Interfaces*, 2011, **3**, 4288.
34 J. Xiao, J. Liang, C. Zhang, Y. Tao, G.-W. Ling and Q.-H. Yang, *Small Methods*, 2018, 1800012.
35 S. Homaeigohar and G. Elbahri, *Materials*, 2014, **7**, 1017.
36 S. Zhang, H. Liu, X. Yin, Z. Li, J. Yu and B. Ding, *Sci. Rep.*, 2017, **7**, 40550.
37 X. Zhao, Y. Li, T. Hua, P. Jiang, X. Yin, J. Yu and B. Ding, *Small*, 2017, **13**, 1603306.

38 J. Lin, B. Ding, J. Yu and Y. Hsieh, *ACS Appl. Mater. Interfaces*, 2010, **2**, 521–528.
39 L. Zhang, Y. Li, J. Yu and B. Ding, *RSC Adv.*, 2015, **5**, 79807.
40 X. Zhao, Y. Li, T. Hua, P. Jiang, X. Yin, J. Yu and B. Ding, *ACS Appl. Mater. Interfaces*, 2017, **9**, 12054.
41 N. Wang, X. Wang, B. Ding, J. Yu and G. Sun, *J. Mater. Chem.*, 2012, **22**, 1445.
42 A. Meireles, E. Giaouris and M. Simoes, *Food Res. Int.*, 2016, **82**, 71.
43 Y. Sun and G. Sun, *Ind. Eng. Chem. Res.*, 2004, **43**, 5015.
44 H. B. Kocer, I. Cerkez, S. D. Worley, R. M. Broughton and T. S. Huang, *ACS Appl. Mater. Interfaces*, 2011, **3**, 3189.
45 P. Cristina, J. M. Antelo, J. Crugeiras and A. Gallego, *J. Phys. Org. Chem.*, 2014, **27**, 407.
46 V. Miri, O. Persyn, J.-M. Lefebvre and R. Seguela, *Eur. Polym. J.*, 2009, **45**, 757.
47 L. T. Asri, M. Crismaru, S. Roest, Y. Chen, O. Ivashenko, P. Rudolf, J. Tiller, H. Mei, T. Loontjens and H. Busscher, *Adv. Funct. Mater.*, 2014, **24**, 346.
48 G. Cado, R. Aslam, L. Seon, T. Garnier, R. Fabre, A. Parat, A. Chassepot, J.-C. Voegel, B. Senger, F. Schneider, Y. Frere, L. Jierry, P. Schaaf, H. Kerdjoudj, M.-H. Metz and F. Boulmedais, *Adv. Funct. Mater.*, 2013, **23**, 4801.
49 X. Li, N. Wang, G. Fan, J. Yu, J. Gao, G. Sun and B. Ding, *J. Colloid Interface Sci.*, 2015, **439**, 12.
50 B. Yeom, E. Shim and B. Pourdeyhimi, *Macromol. Res.*, 2010, **18**, 884.
51 X. Zhao, S. Wang, X. Yin, J. Yu and B. Ding, *Sci. Rep.*, 2016, **6**, 35472.
52 F. Zuo, S. Zhang, H. Liu, H. Fong, X. Yin, J. Yu and B. Ding, *Small*, 2017, **13**, 1702139.
53 Y. Yang, S. Zhang, X. Zhao, J. Yu and B. Ding, *Sep. Purif. Technol.*, 2015, **152**, 14.
54 N. Wang, Y. Yang, S. A. Salem, E. Mohamed, J. Yu and B. Ding, *J. Mater. Chem. A*, 2015, **3**, 23946.
55 W. Leung and C. Hung, *Sep. Purif. Technol.*, 2012, **92**, 174.